J Mater Sci: Mater Electron (2017) 28:2366–2376
DOI 10.1007/s10854-016-5805-6

Synthesis and characterization of nanotree-like polyaniline electrode material for supercapacitors

Runping Jia[1] · Yi Wu[1] · Guangtao Zan[2] · Dongwei Liu[1]

Received: 28 April 2016 / Accepted: 3 October 2016 / Published online: 18 October 2016

Abstract In this work, polyamidoamine (PAMAM) dendrimers are used as templates to synthesize nanotree-like polyaniline (PANI) materials, which are further used as electrode materials for supercapacitors. Effects of PAMAM content on PANIs' structural characteristics and electrochemical properties are investigated detailedly. SEM images show that at 0.1 % PAMAM content, the PANI presents a stable self-assembled dendritic structure composed of many nanorods. Compared with pure PANI, nanotree-like PANI has better crystallinity, higher doping degree, larger high surface area and better reactivity. At a current density of 1 A g^{-1}, the PANI nanotree electrode displays a high specific capacitance value of 812 F g^{-1}, which is 119 % higher than that of pure PANI. Even after 1000 cycles, it still maintains about 69 % of the initial capacitance, showing good electrochemical stability. Thus the PANIs with nanotree structures are promising electrode materials for high-performance electrical energy storage devices. Moreover, the possible electrochemical enhancement mechanism of PANI nanotree electrode for supercapacitor is also discussed.

✉ Runping Jia
jiarp@sit.edu.cn

[1] School of Materials Science and Engineering, Shanghai Institute of Technology, Shanghai 201418, People's Republic of China

[2] Department of Chemistry, Tongji University, Shanghai 200092, People's Republic of China

1 Introduction

Supercapacitors (SCs) as charge-storage devices with the ability to store large amounts of energy with a high power density, excellent reversibility and cycle-ability, are being considered as promising candidates for energy storage [1]. The characteristic performances of SCs are closely related to the physical and chemical features of the electroactive materials that are commonly prepared using conducting polymers, carbons, and metal oxides [2–4]. Among the conducting polymers, PANI has been extensively used as the supercapacitor electrode materials, due to its ease of synthesis, high specific capacitance, good environmental stability, electroactivity, and doping–dedoping chemistry [5–7]. However, PANI's electrochemical performance is unsatisfied under high mass loadings. With an increased mass loading, PANI becomes densely packed and the accessible surface area is decreased, resulting in a limited participation of the conducting polymer in the charge storage process and a comparatively low specific capacitance [8].

To overcome this drawback, several design strategies have been proposed to prepare PANI nanostructures, such as nanotubes [9], nanofibers [8], nanowires [10] and nanorods [11]. For example, Ren et al. [12] prepared PANI nanofibers, nanoflowers, nanorods and nanotubes using an adsorption-template technique, and found that the electrodes' specific capacitances were 521, 543, 638 and 661 F g^{-1} at current density of 1 A g^{-1}, respectively. Yang et al. [13] synthesized hollow PANI nano-capsule with holes on the wall via an interfacial polymerization method, and the specific capacitance of PANI electrode was as high as 502 F g^{-1} at 5 mA cm^{-2}. Based on above-mentioned results, it is also clear that the electrochemical performance of PANI is highly dependent on its shape when its dimension goes down to nanoscale, which is

mainly due to their high surface area, high electrical conductivity and fast ion diffusion process [14, 15]. Thus, it is of significant importance to develop a novel preparation method of the nanostructured PANIs with higher electrochemical performance, well–controlled morphology and structure for efficient access of electrolyte ions. They might be used as electrode materials for the next-generation high-performance electrochemical SCs to meet the future energy-storage demand in hybrid electric vehicles, memory back-up systems, industrial energy management, etc. [1, 16, 17].

Since first reported in 1985 by Tomalia et al. [18], PAMAM dendrimer is characterized as three-dimensional and highly branched polymer with well-defined size and shape. The crowded surface functional groups of higher generations (G > 3) PAMAM dendrimers lead to a close-packed spherical structure surrounding significant interior nanoscale cavities [19]. They can be used as templates and nanoreactors to synthesize nano-clusters or nanocomposite in the field of inorganic metal [20]. Metal ions enter PAMAM nanocavity by electrostatic interactions or complexation reactions [21], then they can be reduced by excess chemical reducing agent to yield nanoparticles [22]. For example, Knecht et al. [23] used PAMAM dendrimers as templates to produce silica nanospheres (30–300 nm). However, there is still no research about the synthesis of organic polymer such as PANI by using PAMAM as available templates, say nothing of its effect on PANI's electrical properties.

In this paper, we use PAMAM as a template to synthesize PANI with a special nanostructure. The as-obtained PANIs' structure, chemical composition and electrochemical performances have been investigated in details. Moreover, the synthesis mechanism is studied preliminary. The proposed PAMAM method can be handily used to synthesize various conducting polymers with special nanostructure, which has a potential application in high-performance electrochemical devices.

2 Experimental

2.1 Materials

Aniline (An, analytical-grade) was first double-distilled in vacuum under nitrogen and then stored in a refrigerator. Other chemicals such as ammonium persulfate (APS), hydrochloric acid (HCl), acetone, and ethanol were all analytical grade and obtained from Sinopharm Chemical Reagent Co. Ltd. Fourth generation amine-terminated PAMAM dendrimer ($G4NH_2$) was used as received from Aldrich Chemical Co. Distilled water was used in the procedure of PANI polymerization.

2.2 Synthesis of PANI nanoparticles

The synthesis of PANI nanoparticles was illustrated in Scheme 1, and the details were as follows: in a typical experiment, appropriate PAMAM (see Table 1) and 100 mL of HCl solution (1 mol L^{-1}) were added into a three-necked round bottomed flask and sonicated for 30 min at room temperature. Then Aniline (0.71 mL) was added and stirred for 30 min and cooled to 0 °C. After that, APS solution (2.28 g APS dissolved in 100 mL of 1 mol L^{-1} HCl aqueous solution) was dropwise added sequentially into the above system under the condition of stirring. A color change of reaction mixture from white to blue even dark green within 8–15 min was observed, indicating the onset of polymerization. The polymerization was allowed to proceed in an ice-water bath for 6 h with continuous stirring. Finally, the products was centrifuged and washed using distilled water, ethanol and acetone for several times to remove impurities and PAMAM, and dried under vacuum at 60 °C for 10 h, the as-obtained dark green powder was named as PANI, which were characterized for further use.

During the synthesis procedure, the chemical oxidation polymerization was proceeded by APS. The PAMAM dissolved in HCl were used as nanoreactors, whose contents strongly affected the structures of PANI nanoparticles. The PANI samples synthesized at different PAMAM contents were summarized in Table 1.

2.3 Characterizations

Fourier transform infrared (FTIR) spectra of the resultant PANI particles were obtained at room temperature with a Nicolet NEXUS870 FTIR spectrometer (USA). Their structures and crystallinities were characterized using a Rigaku D/max2500 X-ray diffractometer (XRD) with CuKα radiation (λ = 1.542 Å, Japan) in the 2θ range of 10°–60°. Their morphologies were observed using a FEI Quanta 200F scanning electron microscope (Holland). The Brunaer-Emmett-Teller (BET) specific surface area, pore volume and pore size were investigated using a ST-08A surface area and pore size analyzers. The electrical conductivities were determined by the four probe method using a Keithley 2400.

2.4 Electrochemical measurements

In a three-electrode system, the electrochemical properties were measured on a CHI660D electrochemical working station in 1.0 mol L^{-1} H_2SO_4 aqueous electrolyte at room temperature. The working electrode was prepared as follows: a viscous slurry containing 90 wt% PANI sample, 5 wt% acetylene black and 5 wt% polytetrafluoroethylene

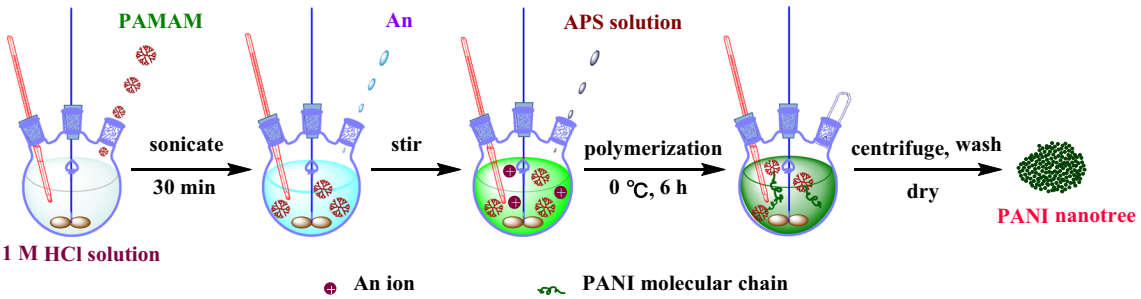

Scheme 1 Synthetic route for PANI nanotree

Table 1 Synthesis of PANIs with different amounts of PAMAM template

PAMAM contents (wt%)	0	0.03	0.05	0.07	0.09	0.10	0.12	0.15
PANIs no.	1#	2#	3#	4#	5#	6#	7#	8#
PANI electrodes no.	1#	2#	3#	4#	5#	6#	7#	8#

(PTFE) was mixed and pressed onto a stainless steel cloth (Mesh sizes 500) current collector at 10 MPa. The as-formed electrodes were then dried overnight at 80 °C in a vacuum oven and denoted as listed in Table 1. Before the electrochemical test, the PANI electrodes were soaked in a 1.0 mol L^{-1} H_2SO_4 solution overnight. The sample loaded on the current collector has a weight of 3–5 mg, and a geometric surface area of about 1 cm^2. A platinum wire and a saturated calomel electrode were used as the counter and reference electrode, respectively. The specific capacitance was calculated from galvanostatic charge–discharge curves according to the following formula:

$$C_s = I \times \Delta t \times m^{-1} \Delta V^{-1}$$

where C_s is the specific capacitance (F g^{-1}), I is the constant discharge current (A), Δt is the time of discharge stage (s), ΔV is the discharge voltage (V) and m is the mass of PANI (g).

In a symmetric two-electrode system, two electrodes with the same PANI loading mass made by above method are separated by a filter paper to form a sandwich structure test system [24]. This sandwich system is soaked in 1 mol L^{-1} H_2SO_4 overnight and sandwiched between two pieces of PTFE plates before the electrochemical test. All electrochemical measurements are carried out on a CHI660D electrochemical working station at room temperature.

3 Results and discussion

3.1 Morphology analysis

SEM images of PANI nanoparticles synthesized under different PAMAM contents are presented in Fig. 1. Clearly, the morphology of PANI without PAMAM is an irregular agglomerate. When PAMAM is introduced into the polymerization procedure, the sizes of PANIs decrease into nanometer scale and show an oriented growth along PAMAM. At 0.1 % PAMAM content, the PANI presents a stable self-assembled dendritic structure together with nanoholes (diameter: ~70 nm), which are composed of lots of nanorods (length: ~90 nm, width: ~25 nm). However, too much PAMAM will make the dendritic structure closer, resulting in a density decrease of nanohole. Here, the dendritic-like PANI with order nanoholes and nanorods can provide a larger liquid–solid interfacial area, which will provide an easy and short path for the ion transport. This kind of PANI electrode material can be beneficial for the capacitance improvement by fast faradic process of PANI electrode.

3.2 Structure analysis

The structures of pure PANI and nano PANIs prepared by the PAMAM template method are further characterized with FTIR and XRD spectra (Figs. 2, 3). For pure PANI, the absorption bands at 3450 and 1300 cm^{-1} are assigned to the stretching vibrations of N–H in aromatic amines and C-N in secondary aromatic amine, respectively. The bands around 1126 and 816 cm^{-1} are originated from the bending vibrations of C–H in–plane and aromatic C–H out of plane. The bands located around 1567 and 1491 cm^{-1} are attributed to the C=C stretching vibrations of the quinonoid (Q) and benzenoid (N) rings, respectively. These characteristic bands confirm the emeraldine chemical structure of the as-obtained PANI [25, 26]. Although the neat PANI and those PANI by PAMAM have similar spectra, the positions and peak intensities of specific bands show differences: the absorption bands at 1300 and 1126 cm^{-1} shift

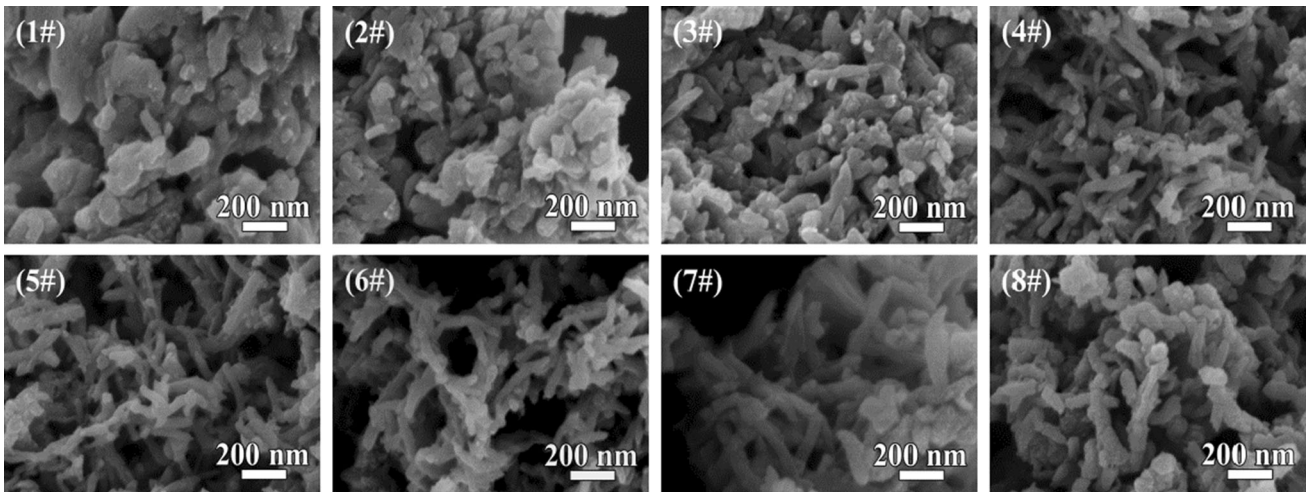

Fig. 1 SEM images of PANIs under varied PAMAM contents

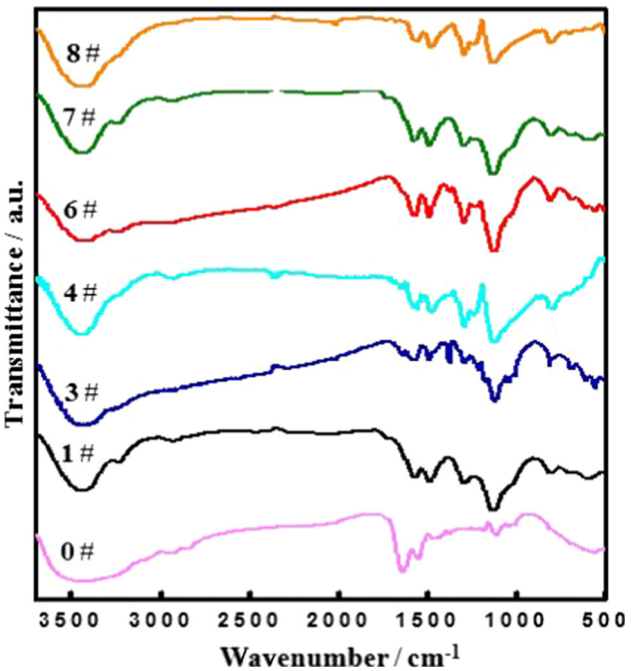

Fig. 2 FTIR spectra of PAMAM ($0^{\#}$) and PANIs under varied PAMAM contents

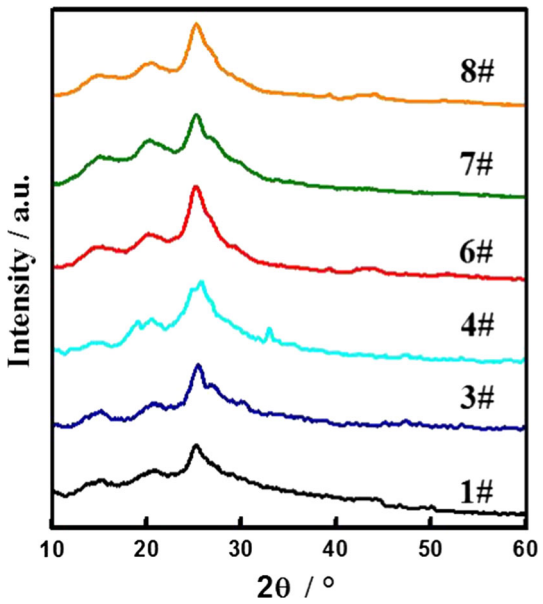

Fig. 3 XRD spectra of PANIs prepared under varied PAMAM contents

to longer wavenumber by 6–8 cm^{-1}, and the intensity of bands at 1567 and 1491 cm^{-1} are dramatically enhanced. The peak shift is due to the polymerization of aniline monomer that is limited into PAMAM's nanocavities, which brings an orderly arrangement in the molecular chain, and leads to an increase of the doping degree of PANI. In this case, the spread of electron cloud of quinone-imine ring occurs in a whole PANI chain through the delocalization of charge, resulting in an enhanced conjugation effect and reduced surface charge density [27, 28]. Due to the doping of PANI leads to the formation of –Q=N^{+}H– groups, the positive charges in the PANI chains increase the dipole moment of the molecule, which should be responsible for the increased strength of 1567 and 1491 cm^{-1} [29].

Figure 3 shows the XRD patterns of PANIs. There are three characteristic diffraction peaks observed at 15.3°, 20.9° and 25.6°. The former arises from the characteristic repeating units and doping diffraction peak of PANI, while the latter two peaks are ascribed to the periodicity parallel and perpendicular to PANI chains, respectively [8, 30]. These peaks display typical emeraldine salt form of amorphous PANI [31]. Meanwhile, with an increasing content of PAMAM, the peak positions of pure PANI and PANIs prepared by PAMAM are almost the same. While their peaks, especially PANI 6#, at 20.9° and 25.6° become

sharper and stronger, and this may be due to the appearance of a relatively ordered structure of the polymer chain. These signify their better crystallinity and highly doping degree [16], which is in good agreement with the SEM results. It is well known that the electrical conductivity improves with the increased degree of crystallinity [32]. So we can expect that the PANIs obtained by PAMAM templates may have better electric properties.

3.3 Specific surface area and pore volume of PANI nanoparticles

In order to investigate the effect of PAMAM on PANI's surface area, we further conducted nitrogen adsorption–desorption and porosity distribution tests. Clearly, all of the PANI samples have high BET surface areas, which are much higher than those of pure PANI and reported PANI samples, and higher average pore diameter than pure PANI, as summarized in Table 2. Such high surface area will be helpful for the spread and reaction of electrolyte ions at PANI/electrolyte interface. At the same time, there are more pore volume with the appropriate pore size, which can facilitate the penetration and transport of electrolytes. These interactions can accelerate the charge flow and lead to the occurrence of a quick faradic redox reaction, so it can be expected that the electrode materials may possess an outstanding specific capacity and rate capability [16, 33–36].

3.4 Electrochemical properties

Research results indicated that the morphologies of the electrode materials strongly influence their capacitance [13, 32, 37, 38]. In order to evaluate the electrochemical characteristics of PANIs as active electrode materials, the cyclic voltammetry and galvanostatic charge–discharge tests are conducted at a potential window of −0.1 to 0.7 V.

3.5 CV analysis

The cyclic voltammetric curves for PANI electrodes are recorded at a scan rate of 1 mV s^{-1} (Fig. 4a). Obviously, two pairs of redox peaks are observed, which come from the redox transformation of the leucoemeraldine–emeraldine (A1/C1) and emeraldine–pernigraniline (A2/C2). This indicates that the current–potential response is potential dependent, and the pseudocapacitance mainly derives from the redox reaction of PANIs [16, 34]. Obviously, the absolute areas of all nano PANI electrodes are much higher than that of pure electrode (PANI 1#). The PANI 6# reaches the maximum value (∼1.33) that is higher by 343 % than that of pure PANI electrode (∼0.30), displaying the highest capacitance. Since the PANI 6# shows a stable nanotree structure with lots of nanoholes and the highest surface area, the ionic transport and diffusion are greatly enhanced [26]. Based on this phenomenon, we infer that PANI's morphology strongly influences the redox transition of leucoemeraldine form (semiconductor)/polaronic emeraldine form (conductor) and faradaic transformation of emeraldine/pernigraniline.

Figure 4b shows the CV curves of PANI 6# electrode at different scan rates (1–50 mV s^{-1}). It's clear that the cathodic peaks (A1, A2) shift positively, while the anodic peaks (C1, C2) shift negatively, for which the internal resistance of the electrode is responsible [26]. Compared with the CV loops of PANI 6# electrode at 1 mV s^{-1}, the two pairs of redox peaks at 50 mV s^{-1} are hardly observed. This indicates that the PANI electrode has poor

Table 2 BET results of PANI nanoparticles by PAMAM template method

PANI no.	Methods	Surface area (m^2 g^{-1})	Average pore size (nm)	Pore volume (cm^3 g^{-1})
PANI 1#	Our method	17.79	7.05	0.12
PANI 3#	Our method	38.47	11.80	0.22
PANI 4#	Our method	59.89	14.96	0.21
PANI 6#	Our method	87.14	17.69	0.20
PANI 7#	Our method	62.37	15.86	0.19
PANI 8#	Our method	48.53	12.05	0.15
PANI nanofibers [33]	Interfacial polymerization	37.2–54.6	–	–
PANI nanofibers [34]	In situ oxidative polymerization	33.6	8.3	0.2
PANI nanoparticles [35]	In situ oxidative polymerization	36.96–53.11	127.46–174.58	0.12–0.23
PANI [36]	In situ oxidative polymerization	17.59	32.54	0.14
PANI nanospheres [16]	In situ oxidative polymerization	67.9	11.5	–
PANI nanotubes [16]	In situ oxidative polymerization	77.1	18	–
PANI nanofibers [16]	In situ oxidative polymerization	30.9	16.3	–

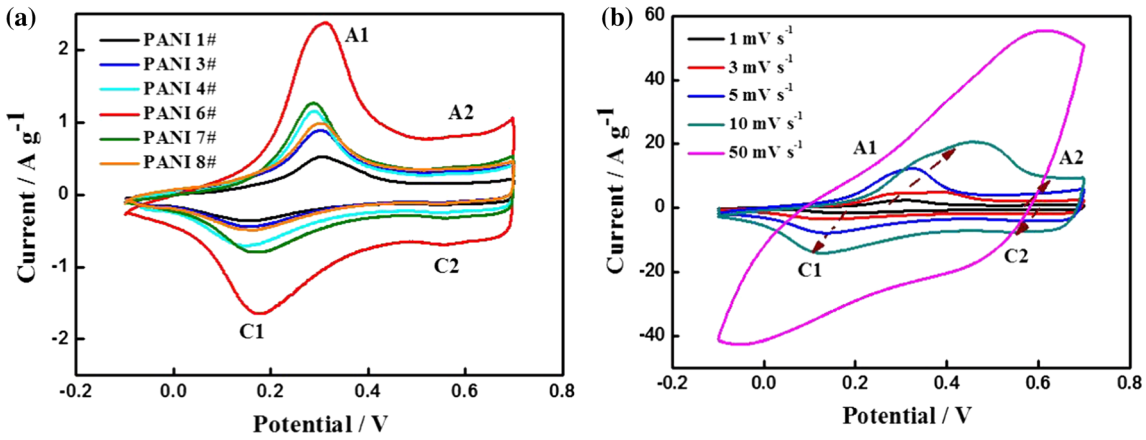

Fig. 4 CV curves of PANI electrodes. **a** Different PANI electrodes at the scan rate of 1 mV s^{-1}, **b** PANI 6# electrode at different scan rates

reversibility, which might be due to the pseudocapacitance characteristic of PANI materials [39]. Even at 50 mV s^{-1}, the CV loop of PANI 6# electrode still shows the largest integrated area, suggesting its remarkable capacitance and fastest ionic transportation rate [13].

3.6 GCD analysis

The galvanostatic charge–discharge measurements are carried out on as-obtained PANI electrodes (Fig. 5). It's seen that all the curves are not ideal straight line, suggesting the process of a faradic reaction. Moreover, the potential responses of these electrodes during charge and discharge are nearly symmetrical, which is a characteristic capacitive behavior and excellent reversibility of PANI electrode [26].

Figure 5a shows the comparison of GCD curves for PANI electrodes at a current density of 1 A g^{-1}. Clearly, the discharge times of PANI electrodes by PAMAM are longer than that of pure PANI, displaying a significant improvement of specific capacitance. In order to investigate the effect of conductivity on electrode performance, the voltage drop (IR drop) in charge–discharge curve of all PANI electrodes are recorded (see Table 3). Clearly, with an increased conductivity, the IR drop decreases slightly, and the value of PANI 6# electrode is the lowest, which is consistent with the aforementioned BET and CV results.

To further investigate the rate capability of PANI electrode, the charge–discharge curves of PANI 6# electrode are recorded at different current density from 1 to 10 A g^{-1} (Fig. 5b). It's seen that with the increase of current density, the discharge time decreases distinctly. According to the discharge time of GCD curves, the specific capacitance is calculated. At low current density of 1 A g^{-1}, it's as high as 812 F g^{-1}. With increasing current density, it decreases gradually. At 10 A g^{-1}, the specific capacitance is 656 F g^{-1}, showing a capacity retention rate of 81 %. This might be because that high current density drastically slows down the diffusion rate of electrolyte, and thus the ions can only penetrate into the outer surface of the nanostructures,

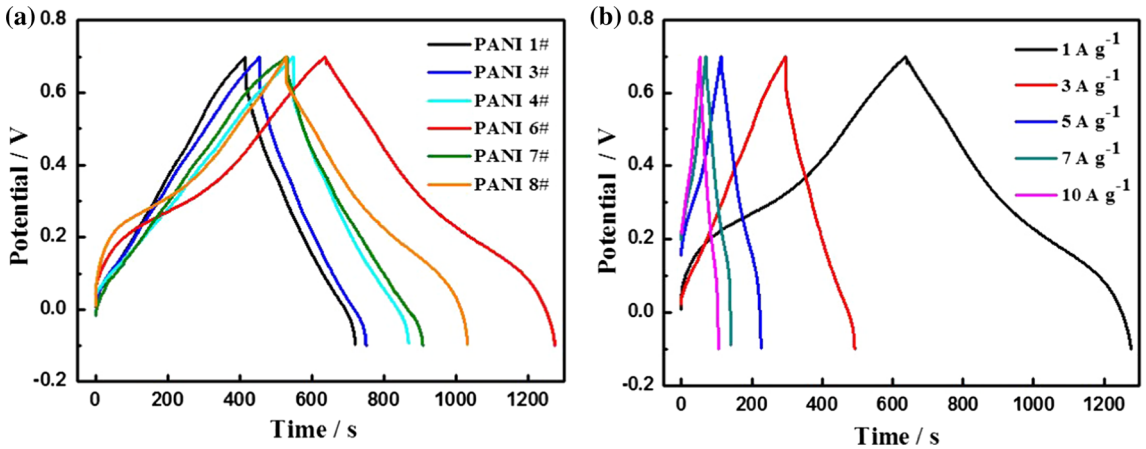

Fig. 5 GCD curves of the PANI electrodes. **a** Different PANI electrodes at current density of 1 A g^{-1}, **b** PANI 6# electrode at different current densities

Table 3 Conductivity and IR drop of PANIs with the different quantity of PAMAM as template

PANIs	PANI 1#	PANI 3#	PANI 4#	PANI 6#	PANI 7#	PANI 8#
Conductivity (S cm^{-1})	1.6	1.8	2.6	5.8	2.8	2.1
IR drop (V)	0.075	0.068	0.061	0.005	0.034	0.073

which in turn decrease the active surface area of the electrode material taking part in the charge–discharge process [40].

Figure 6 shows the specific capacitances of PANI electrodes. Under a given current density of 1–10 A g^{-1}, the specific capacitances of nano PANI electrodes are much higher than pure PANI electrode, and the value of PANI 6# electrode reaches the maximum. Since the PANI 6# electrode is prepared by a stable self-assembled dendritic structure together with higher surface area, which can provide more contact surface for electrochemical reaction, and then make the ion penetration into the inner surface of active electrode material easier. This will be helpful to get a higher specific capacitance and a better rate performance, which is of great importance during charging–discharging process in energy storing devices.

3.7 EIS analysis

Commonly, the EIS experiments are used to study the electrochemical behavior of the electrodes at the electrode/electrolyte interface. Here Nyquist plots for PANI electrodes are shown in Fig. 7. The semicircle portion observed at higher frequencies corresponds to the electron-transfer-limited process, whereas the linear part is characteristic of the lower frequencies range and represents the diffusion-limited electrode process [41]. The intersection point at the Z′ axis represents the solution resistance (Rs), and the diameter of the semicircle reflects the charge transport resistance (Rct) (inset in Fig. 7). Because the Rs is insensitive to the electrode surface, the PANI electrodes have almost the same Rs (1.31 Ω) [13]. However, the nano PANI electrodes have lower Rct value when compared with that of pure PANI (16.15 Ω), and the Rct value of PANI 6# electrode is the lowest (3.39 Ω). Moreover, the vertical shape at lower frequencies indicates a pure capacitive behavior. The more vertical the curve is, the more closely the supercapacitor behaves as an ideal capacitor [24]. The most vertical line at low frequency region of PANI 6# indicates its more ideal capacitive property, which may be due to the synergistic effect of special morphology, high crystallinity and doping degrees, large specific surface area and appropriate pore size distribution [26]. This might be because PANI's nanostructures benefit ions transfer between the solution and the electrode active center, as well as the fast and reversible faradic reaction on PANI nanotree electrode [42, 43], which is in good accordance with aforementioned CV and GCD results.

3.8 Cycling ability test

To further study the cyclic stability of PANI electrodes, the endurance galvanostatic charge–discharge experiments are also carried out at a current density of 1 A g^{-1} (see Fig. 8). After 1000 consecutive cycles, the retention rate of pure PANI electrode is only 35 % of its original specific capacitance. However, the rate can be as high as about 65 % for PANI nanoparticles, even up to 69 % for PANI 6# electrode. The decrease of specific capacitance might be due to parts of the PANI ordered structures being broken by repeated transfer of ions [44]. For PANI nanoparticles, the extent of PANI structure swelling and shrinking is

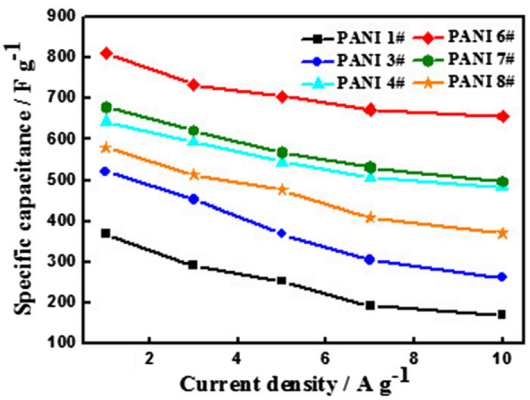

Fig. 6 Specific capacitance plots of PANI electrodes at different current densities

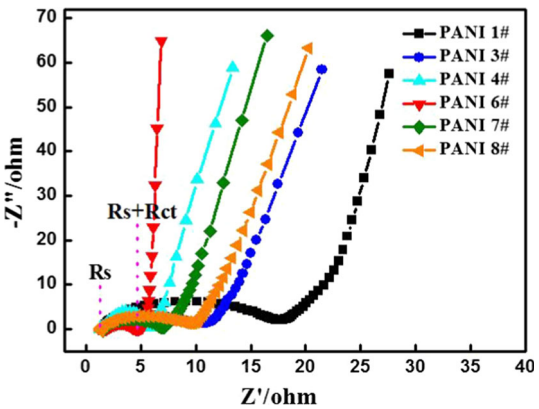

Fig. 7 EIS plots of PANI electrodes measured at frequency range of 100 kHz–0.01 Hz at the open-circuit potential

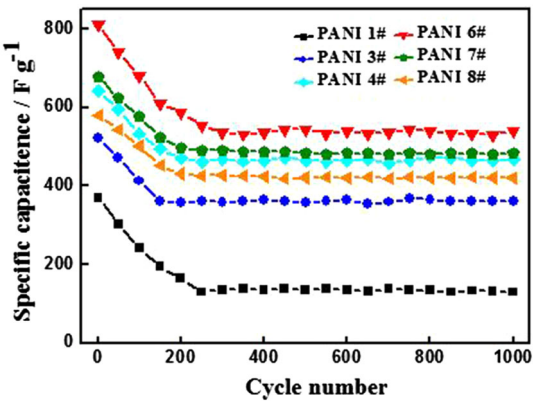

Fig. 8 Cycling stability of PANI electrodes in the voltage range of −0.1 to 0.7 V

obviously relaxed during the charge–discharge process, resulting in a higher retention rate [45, 46].

To provide the best indication of an electrode performance for industrial applications, a symmetric two-electrode supercapacitor was assembled and tested. Since the PANI 6# electrode shows the best electrochemical properties, it is chosen as active electrode materials for the two-electrode tests. The CV plots show that the symmetric supercapacitor has a relatively wide potential window of 1.0 V (Fig. 9a). These plots have similar shape with redox peaks even at a very high scan rate, demonstrating the good conductivity and the good capacitive behavior of assembled electrodes. The GCD plots show symmetric shape, indicating the good reversibility of the charge–discharge process (Fig. 9b). It should be noted that the GCD plots show nonlinear shape, and this is consistent with the results of CV plots that redox reaction happened during the charge and discharge process. The specific capacity of the symmetric SCs based on the weight of both electrodes is calculated to be 92.5, 91.5, 79.0, 78.9, 78.8, 77.2 F g^{-1} at the current density of 0.5, 1.0, 2.0, 5.0, 10.0, 20.0 A g^{-1} according to the GCD plots. The EIS plot shows that the symmetric supercapacitor has a very low equivalent series resistance of about 1.5 Ω (Fig. 9c), and it is an important factor in determining the power density of the device [24, 47]. The ragone plot of the device is calculated by the GCD results (Fig. 9d). The device has a maximum energy density of 12.68 W h kg^{-1} at 0.5 A g^{-1} and a maximum power density of 2836 W kg^{-1} at 20 A g^{-1}, exhibiting potential for practical application in SCs.

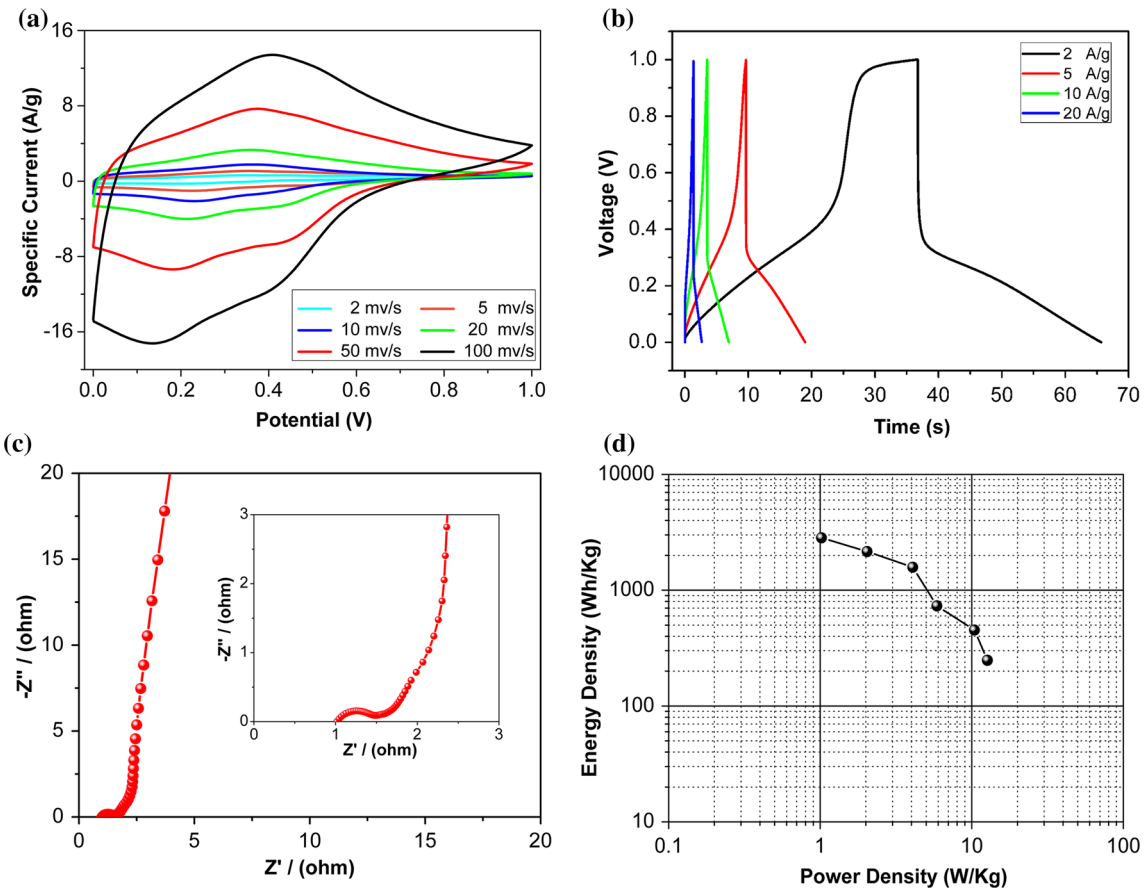

Fig. 9 **a** CV plots, **b** GCD plots, **c** EIS plot and **d** ragone plot of the symmetric PANI 6# two-electrode system at different scan rates in 1.0 mol L^{-1} aqueous H_2SO_4 electrolyte

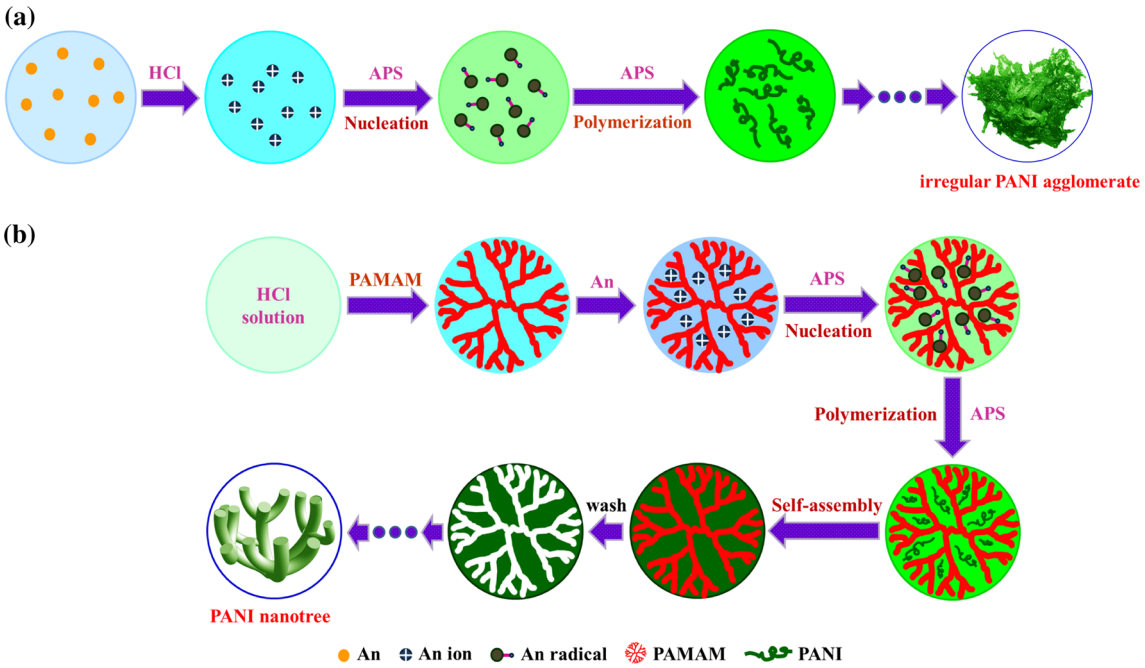

Fig. 10 Schematic drawing of synthesis mechanism of PANI (**a**) and PANI nanotree (**b**)

3.9 Possible electrochemical enhancement mechanism of supercapacitor electrode material prepared by PANI nanotree

Based on above-obtained results, it's clear that the supercapacitor electrode material prepared by PANI nanomaterials especially nanotree has better comprehensive electrochemical characteristics. Both of its special tree-like nanostructure and high surface area should be responsible for this improvement. Here, possible electrochemical enhancement mechanism of PANI nanotree is illustrated briefly. As seen in Fig. 10a, aniline monomer in HCl solution presents as ionic form. When APS molecules are introduced into the system, they can form lots of free radicals driven by electromotive force, which can further induce the oxidative polymerization of aniline monomer. Since the APS molecules are uniformly distributed in the whole solution, the PANI molecular chains grow from every direction, finally resulting in an unordered arrangement of PANI microscale structure with less accessible surface area. Thus the penetration of electroactive ions far inside the PANI is limited and the utilization of the conducting polymer in the charge storage process is reduced [8]. So the disordered structure of PANI have low electrochemical performance. However, when the PAMAM is used as a nanotemplate in this system (Fig. 10b), the polymerization reaction of aniline monomer is limited in the nanoscale cavities of PAMAM due to the strong interaction such as hydrogen bond and electrostatic interactions [21]. Hence the PANI molecular chains can only grow along the PAMAM dendrimer direction, resulting in a stable and ordered PAMAM–PANI composite. Since PAMAM can be easily removed by organic solvent, pure and stable PANI nanotree together with lots of nanocavies can be finally obtained. Here the PAMAM dendrimer template can not only precisely control the size and shape of the nano-PANI, but also give it a high specific surface area, which facilitates the effective penetration of the electrolyte and ensures high utilization of the conducting polymer [8]. Both of these interactions lead to the electrochemical enhancement of supercapacitor electrode prepared by PANI nanotree.

4 Conclusions

In summary, the ordered nanotree-like PANI with a diameter of 25 nm and length of about 90 nm are synthesized using 0.1 % PAMAM as a template. It shows a good capacitive performance due to its particular structure. Its specific capacitance is as high as 812 F g^{-1}, and it can maintain about 69 % of the initial capacitance even after 1000 cycles, which is attributed to a larger effective surface area. The above results displayed that this low-cost and environment friendly nanostructured PANI tree can be a promising electrode material for capacitors. Importantly, this special templating approach provides a new route for the synthesis and fabrication of other electrode materials in supercapacitor applications.

Acknowledgments The authors gratefully acknowledge the financial support of the National Science Youth Foundation (21106083), Shanghai Leading Academic Discipline Project (J51504), Shanghai Innovation action plan project (15520503400), Shanghai Teacher Professional Development project (201456) and Composite Materials Leading Academic Discipline Project from Shanghai Institute of Technology (10210Q140001).

References

1. J.R. Miller, P. Simon, Electrochemical capacitors for energy management. Sci. Mag. **321**(5889), 651–652 (2008)
2. W.J. Zhou, D.D. Zhao, M.W. Xu, C.L. Xu, H.L. Li, Effects of the electrodeposition potential and temperature on the electrochemical capacitance behavior of ordered mesoporous cobalt hydroxide films. Electrochim. Acta **53**(24), 7210–7219 (2008)
3. P. Simon, Y. Gogotsi, Materials for electrochemical capacitors. Nat. Mater. **7**(11), 845–854 (2008)
4. S.L. Chou, J.Z. Wang, S.Y. Chew, H.K. Liu, S.X. Dou, Electrodeposition of MnO_2 nanowires on carbon nanotube paper as free-standing, flexible electrode for supercapacitors. Electrochem. Commun. **10**(11), 1724–1727 (2008)
5. A.G. MacDiarmid, J.C. Chiang, A.F. Richter, Polyaniline: a new concept in conducting polymers. Synthetic Met. **18**(1), 285–290 (1987)
6. D. Li, J.X. Huang, R.B. Kaner, Polyaniline nanofibers: a unique polymer nanostructure for versatile applications. Accounts Chem. Res. **42**(1), 135–145 (2008)
7. E.T. Kang, K.G. Neoh, K.L. Tan, Polyaniline: a polymer with many interesting intrinsic redox states. Prog. Polym. Sci. **23**(2), 277–324 (1998)
8. Y.E. Miao, W. Fan, D. Chen, T.X. Liu, High-performance supercapacitors based on hollow polyaniline nanofibers by electrospinning. ACS Appl. Mater. Inter. **5**(10), 4423–4428 (2013)
9. Z.M. Zhang, M.X. Wan, Y. Wei, Highly crystalline polyaniline nanostructures doped with dicarboxylic acids. Adv. Funct. Mater. **16**(8), 1100–1104 (2006)
10. K. Wang, J.Y. Huang, Z.X. Wei, Conducting polyaniline nanowire arrays for high performance supercapacitors. J. Phys. Chem. C **114**(17), 8062–8067 (2010)
11. X.L. Bai, X.T. Li, N. Li, Y. Zuo, L.F. Wang, J.X. Li, S.L. Qiu, Synthesis of cluster polyaniline nanorod via a binary oxidant system. Mat. Sci. Eng. C **27**(4), 695–699 (2007)
12. L.J. Ren, G.N. Zhang, J.F. Wang, L.P. Kang, Z.B. Lei, Z.W. Liu, Z.T. Liu, Z.P. Hao, Z.H. Liu, Adsorption–template preparation of polyanilines with different morphologies and their capacitance. Electrochim. Acta **145**, 99–108 (2014)
13. W.L. Yang, Z. Gao, N.N. Song, Y.Y. Zhang, Y.C. Yang, J. Wang, Synthesis of hollow polyaniline nano-capsules and their supercapacitor application. J. Power Sources **272**, 915–921 (2014)
14. J.L. Liu, M.Q. Zhou, L.Z. Fan, P. Li, X.H. Qu, Porous polyaniline exhibits highly enhanced electrochemical capacitance performance. Electrochim. Acta **55**(20), 5819–5822 (2010)
15. Z. Mandić, M.K. Roković, T. Pokupčić, Polyaniline as cathodic material for electrochemical energy sources: the role of morphology. Electrochim. Acta **54**(10), 2941–2950 (2009)
16. W. Chen, R.B. Rakhi, H.N. Alshareef, Morphology-dependent enhancement of the pseudocapacitance of template-guided tunable polyaniline nanostructures. J. Phys. Chem. C **117**(29), 15009–15019 (2013)
17. J.L. Shen, C.Y. Yang, X.W. Li, G.C. Wang, High-performance asymmetric supercapacitor based on nanoarchitectured polyaniline/graphene/carbon nanotube and activated graphene electrodes. ACS Appl. Mater. Inter. **5**(17), 8467–8476 (2013)
18. D.A. Tomalia, H. Baker, J. Dewald, M. Hall, G. Kallos, S. Martin, J. Roeck, J. Ryder, P. Smith, A new class of polymers: starburst-dendritic macromolecules. Polym. J. **17**(1), 117–132 (1985)
19. P.K. Maiti, T. Çağın, G.F. Wang, W.A. Goddard, Structure of PAMAM dendrimers: generations 1 through 11. Macromolecules **37**(16), 6236–6254 (2004)
20. B.L. Frankamp, A.K. Boal, M.T. Tuominen, V.M. Rotello, Direct control of the magnetic interaction between iron oxide nanoparticles through dendrimer-mediated self-assembly. J. Am. Chem. Soc. **127**(27), 9731–9735 (2005)
21. K. Esumi, R. Isono, T. Yoshimura, Preparation of PAMAM- and PPI-metal (silver, platinum, and palladium) nanocomposites and their catalytic activities for reduction of 4-nitrophenol. Langmuir **20**(1), 237–243 (2004)
22. R.W.J. Scott, O.M. Wilson, R.M. Crooks, Synthesis, characterization, and applications of dendrimer-encapsulated nanoparticles. J. Phys. Chem. B **109**(2), 692–704 (2005)
23. M.R. Knecht, S.L. Sewell, D.W. Wright, Size control of dendrimer-templated silica. Langmuir **21**(5), 2058–2061 (2005)
24. Y.F. Xu, I. Hennig, D. Freyberg, A.J. Strudwick, M.G. Schwab, T. Weitz, K.C. Cha, Inkjet-printed energy storage device using grapheme/polyaniline inks. J. Power Sources **248**(4), 483–488 (2014)
25. H. Guan, L.Z. Fan, H.C. Zhang, X.H. Qu, Polyaniline nanofibers obtained by interfacial polymerization for high-rate supercapacitors. Electrochim. Acta **56**(2), 964–968 (2010)
26. W. Chen, R.B. Rakhi, H.N. Alshareef, Facile synthesis of polyaniline nanotubes using reactive oxide templates for high energy density pseudocapacitors. J. Mater. Chem. A **1**(10), 3315–3324 (2013)
27. W. Liu, A.L. Cholli, R. Nagarajan, J. Kumar, S. Tripathy, F.F. Bruno, L. Samuelson, The role of template in the enzymatic synthesis of conducting polyaniline. J. Am. Chem. Soc. **121**(49), 11345–11355 (1999)
28. D.H. Zhou, Y.H. Li, J.Y. Wang, P. Xu, X.J. Han, Synthesis of polyaniline nanofibers with high electrical conductivity from CTAB–SDBS mixed surfactants. Mater. Lett. **65**(23), 3601–3604 (2011)
29. P.S. Rao, S. Subrahmanya, D.N. Sathyanarayana, Inverse emulsion polymerization: a new route for the synthesis of conducting polyaniline. Synthetic Met. **128**(3), 311–316 (2002)
30. Q. Yan, M.Y. Wang, Y.H. Wu, Q. Shen, Tea polyphenol as environmentally friendly dopant and thermal stabilizer for polyaniline. Mater. Lett. **170**, 202–204 (2016)
31. Y.B. Zhao, M. Arowo, W. Wu, J.F. Chen, Effect of additives on the properties of polyaniline nanofibers prepared by high gravity chemical oxidative polymerization. Langmuir **31**(18), 5155–5163 (2015)
32. W. Łużny, E. Bańka, Relations between the structure and electric conductivity of polyaniline protonated with camphorsulfonic acid. Macromolecules **33**(2), 425–429 (2000)
33. J.X. Huang, R.B. Kaner, A general chemical route to polyaniline nanofibers. J. Am. Chem. Soc. **126**(3), 851–855 (2004)
34. H.L. Xu, X.W. Li, G.C. Wang, Polyaniline nanofibers with a high specific surface area and an improved pore structure for supercapacitors. J. Power Sources **294**, 16–21 (2015)
35. Q. Qin, J. Tao, Y. Yang, X. Dong, In situ oxidative polymerization of polyaniline counter electrode on ITO conductive glass substrate. Polym. Eng. Sci. **51**(4), 663–669 (2011)
36. X.L. Li, Q.N. Zhong, X.L. Zhang, T.T. Li, J.M. Huang, In-situ polymerization of polyaniline on the surface of graphene oxide for high electrochemical capacitance. Thin Solid Films **584**, 348–352 (2015)

37. H.W. Park, T. Kim, J. Huh, M. Kang, J.E. Lee, H. Yoon, Anisotropic growth control of polyaniline nanostructures and their morphology-dependent electrochemical characteristics. ACS Nano **6**(9), 7624–7633 (2012)
38. Y. Gu, J.W. Cai, M.Z. He, L.P. Kang, Z.B. Lei, Z.H. Liu, Preparation and capacitance behavior of manganese oxide hollow structures with different morphologies via template-engaged redox etching. J. Power Sources **239**, 347–355 (2013)
39. S.J. He, X.W. Hu, S.L. Chen, H. Hu, M. Hanif, H.Q. Hou, Needle-like polyaniline nanowires on graphite nanofibers: hierarchical micro/nano-architecture for high performance supercapacitors. J. Mater. Chem. **22**(11), 5114–5120 (2012)
40. H. Lee, J. Kang, M.S. Cho, J.B. Choi, Y.K. Lee, MnO_2/graphene composite electrodes for supercapacitors: the effect of graphene intercalation on capacitance. J. Mater. Chem. **21**(45), 18215–18219 (2011)
41. L.P. Zheng, X.Y. Wang, H.F. An, X.Y. Wang, L.H. Yi, L. Bai, The preparation and performance of flocculent polyaniline/carbon nanotubes composite electrode material for supercapacitors. J. Solid State Electr. **15**(4), 675–681 (2011)
42. Z.B. Lei, J.T. Zhang, X.S. Zhao, Ultrathin MnO_2 nanofibers grown on graphitic carbon spheres as high-performance asymmetric supercapacitor electrodes. J. Mater. Chem. **22**(1), 153–160 (2012)
43. L.L. Zhang, X. Zhao, M.D. Stoller, Y.W. Zhu, H.X. Ji, S. Murali, Y.P. Wu, S. Perales, B. Clevenger, R.S. Ruoff, Highly conductive and porous activated reduced graphene oxide films for high-power supercapacitors. Nano Lett. **12**(4), 1806–1812 (2012)
44. Y.Q. Huo, H.Y. Zhang, J.Y. Jiang, Y. Yang, A three-dimensional nanostructured PANI/MnO_x porous microsphere and its capacitive performance. J. Mater. Sci. **47**(19), 7026–7034 (2012)
45. G. Lota, K. Fic, E. Frackowiak, Carbon nanotubes and their composites in electrochemical applications. Energy Environ. Sci. **4**(5), 1592–1605 (2011)
46. G.X. Wang, Q.Q. Tang, H. Bao, X.W. Li, G.C. Wang, Synthesis of hierarchical sulfonated graphene/MnO_2/polyaniline ternary composite and its improved electrochemical performance. J. Power Sources **241**, 231–238 (2013)
47. Y.F. Xu, M.G. Schwab, A.J. Strudwick, I. Hennig, X.L. Feng, Z.S. Wu, K. Müllen, Screen-printable thin film supercapacitor device utilizing graphene/polyaniline inks. Adv. Energy Mater. **3**(8), 1035–1040 (2013)